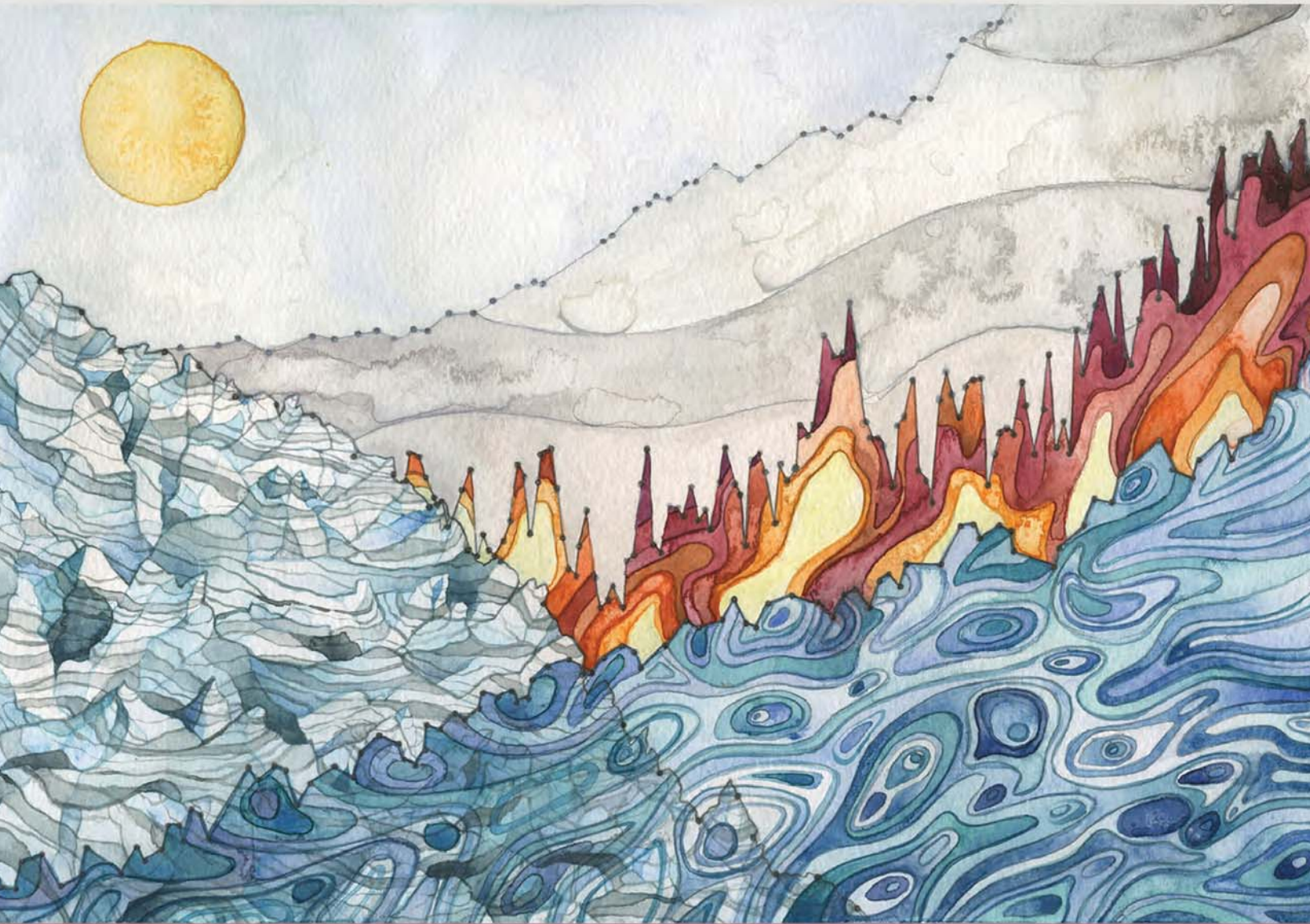


STATE OF THE CLIMATE IN 2015



Special Supplement to the
Bulletin of the American Meteorological Society
Vol. 97, No. 8, August 2016

for 1993–2015 are $0.19 (\pm 0.09) \text{ W m}^{-2}$ from 700 to 2000 m, $0.24 (\pm 0.04) \text{ W m}^{-2}$ from 700 to 1800 m, and $0.19 (\pm 0.08) \text{ W m}^{-2}$ from 700 to 2000 m for the MRI/JMA, PMEL/JPL/JIMAR, and NCEI estimates, respectively. Here, 5%–95% uncertainty estimates for the trends are based on the residuals, taking their temporal correlation into account when estimating degrees of freedom (Von Storch and Zwiers 1999). For 2000–6000 m, the linear trends are about $0.07 (\pm 0.04) \text{ W m}^{-2}$ (again at 5%–95% uncertainty) from 1992 to 2009 (update of Purkey and Johnson 2010; D. Desbruyères and S. G. Purkey, 2016, personal communication).

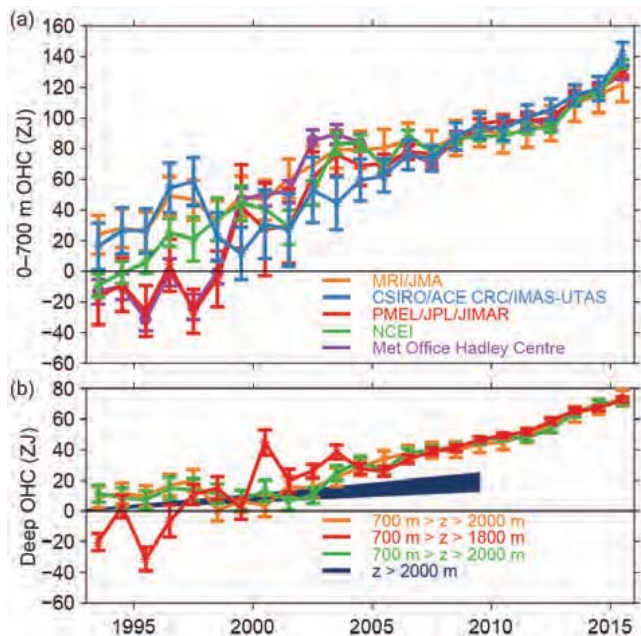


FIG. 3.6. (a) Time series of annual average global integrals of in situ estimates of upper (0–700 m) OHCA ($1 \text{ ZJ} = 10^{21} \text{ J}$) for 1993–2015 with standard errors of the mean. The MRI/JMA estimate is an update of Ishii and Kimoto (2009). The CSIRO/ACE CRC/IMAS-UTAS estimate is an update of Domingues et al. (2008). The PMEL/JPL/JIMAR estimate is an update of Lyman and Johnson (2014). The NCEI estimate follows Levitus et al. (2012). The Met Office Hadley Centre estimate is computed from gridded monthly temperature anomalies (relative to 1950–2015) following Palmer et al. (2007). See Johnson et al. (2014) for more details on uncertainties, methods, and datasets. For comparison, all estimates have been individually offset (vertically on the plot), first to their individual 2005–15 means (the best sampled time period), and then to their collective 1993 mean. (b) Time series of annual average global integrals of in situ estimates of intermediate (700–2000 m for MRI/JMA and NCEI, 700–1800 m for PMEL/JPL/JIMAR) OHCA for 1993–2015 with standard errors of the mean, and a long-term trend with one standard error uncertainty shown from 1992–2009 for deep and abyssal ($z > 2000 \text{ m}$) OHCA updated (D. Desbruyères and S. G. Purkey, 2016, personal communication) following Purkey and Johnson (2010).

Summing the three layers, the full-depth ocean heat gain rate ranges from 0.52 to 0.74 W m^{-2} .

d. **Salinity**—G. C. Johnson, J. Reagan, J. M. Lyman, T. Boyer, C. Schmid, and R. Locarnini

1) **INTRODUCTION**—G. C. Johnson and J. Reagan

Salinity patterns, both long-term means and their variations, reflect ocean storage and transport of freshwater, a key aspect of global climate (e.g., Rhein et al. 2013). Ocean salinity distributions are largely determined by patterns of evaporation, precipitation, and river runoff (e.g., Schanze et al. 2010), and in some high-latitude regions, sea ice formation, advection, and melt (e.g., Petty et al. 2014). The result is relatively salty sea surface salinity (SSS) values in the subtropics, where evaporation dominates, and fresher SSS values under the intertropical convergence zones (ITCZs) and in the subpolar regions, where precipitation dominates. These fields are further modified by ocean advection (e.g., Yu 2011). In the subsurface, fresher subpolar waters slide along isopycnals to intermediate depths, underneath saltier subtropical waters, which are in turn capped at low latitudes by fresher tropical waters (e.g., Skliris et al. 2014). Salinity changes in these layers quantify the increase of the hydrological cycle with global warming over the recent decades, likely more accurately and directly than evaporation and precipitation estimates (Skliris et al. 2014). Below that, the salty North Atlantic Deep Waters formed mostly by open ocean convection are found, with salinities that vary over decades (e.g., van Aken et al. 2011). Fresher and colder Antarctic Bottom Waters, formed mostly in proximity to ice shelves, fill the abyss of much of the ocean (Johnson 2008), freshening in recent decades (e.g., Purkey and Johnson 2013). Salinity changes also have an effect on sea level (e.g., Durack et al. 2014) and the thermohaline circulation (e.g., Kuhlbrodt et al. 2007).

To investigate interannual changes of subsurface salinity, all available subsurface salinity profile data are quality controlled following Boyer et al. (2013) and then used to derive 1° monthly mean gridded salinity anomalies relative to a long-term monthly mean for years 1955–2006 (World Ocean Atlas 2009; Antonov et al. 2010) at standard depths from the surface to 2000 m (Boyer et al. 2012). In recent years, the single largest source of salinity profiles for the world’s ocean is the Argo program with its fleet of profiling floats (Riser et al. 2016). These data are a mix of real-time (preliminary) and delayed-mode (scientific quality controlled). Hence, the estimates presented here could change after all data have been subjected to scientific quality control. The SSS analysis relies on Argo in situ

data downloaded in January 2016, with annual maps generated following Johnson and Lyman (2012) as well as monthly maps from BASS (Xie et al. 2014), a bulk (as opposed to skin) SSS data product that blends in situ SSS data with data from the Aquarius (Le Vine et al. 2014) and SMOS (Soil Moisture and Ocean Salinity; Font et al. 2013) satellite missions. The Aquarius mission ended in June 2015, leaving SMOS as the sole source for satellite SSS for the rest of 2015. BASS maps can be biased fresh around land (including islands) and should be compared carefully with in situ data-based maps at high latitudes before trusting features there. Salinity is measured as a dimensionless quantity and reported on the 1978 Practical Salinity Scale, or PSS-78 (Fofonoff and Lewis 1979). Surface salinity values in the open ocean range from about 32 to 37.5, with seasonal variations exceeding 1 in a few locations (Johnson et al. 2012).

2) SEA SURFACE SALINITY (SSS)—G. C. Johnson and J. M. Lyman

The 2015 SSS anomalies (Fig. 3.7a, colors) reveal some large-scale patterns that largely held from 2004 to 2014 (e.g., Johnson et al. 2015b, and previous *State of the Climate* reports.). Regions around the subtropical salinity maxima are generally salty with respect to *World Ocean Atlas (WOA) 2009* (Antonov et al. 2010). Most of the high latitude, low-salinity regions appear fresher overall than *WOA 2009*, both in the vicinity of much of the Antarctic Circumpolar Current near 50°S and in portions of the subpolar gyres of the North Pacific and North Atlantic. These multiyear patterns are consistent with an increase in the hydrological cycle (that is, more evaporation in drier locations and more precipitation in rainy areas) over the ocean expected in a warming climate (Rhein et al. 2013). The large, relatively fresh patch in 2015 west of Australia and the Indonesian Throughflow was more prominent in previous years back to 2011 (Johnson and Lyman 2012). Its origin is associated with the strong 2010–12 La Niña and other climate indices (Fasullo et al. 2013; Johnson et al. 2015b).

Sea surface salinity changes from 2014 to 2015 (Fig. 3.7b, colors) strongly reflect 2014 anomalies in evaporation minus precipitation (see Fig. 3.12). Advection by anomalous ocean currents (see Fig. 3.19) also plays a role in SSS changes. The most prominent large-scale SSS changes from 2014 to 2015 were freshening under the Pacific ITCZ and salinification in the tropical warm pool around the Maritime Continent (Fig. 3.7b). The freshening is associated with stronger-than-usual freshwater fluxes into the ocean under the ITCZ (see Fig. 3.12) and anomalous eastward flow

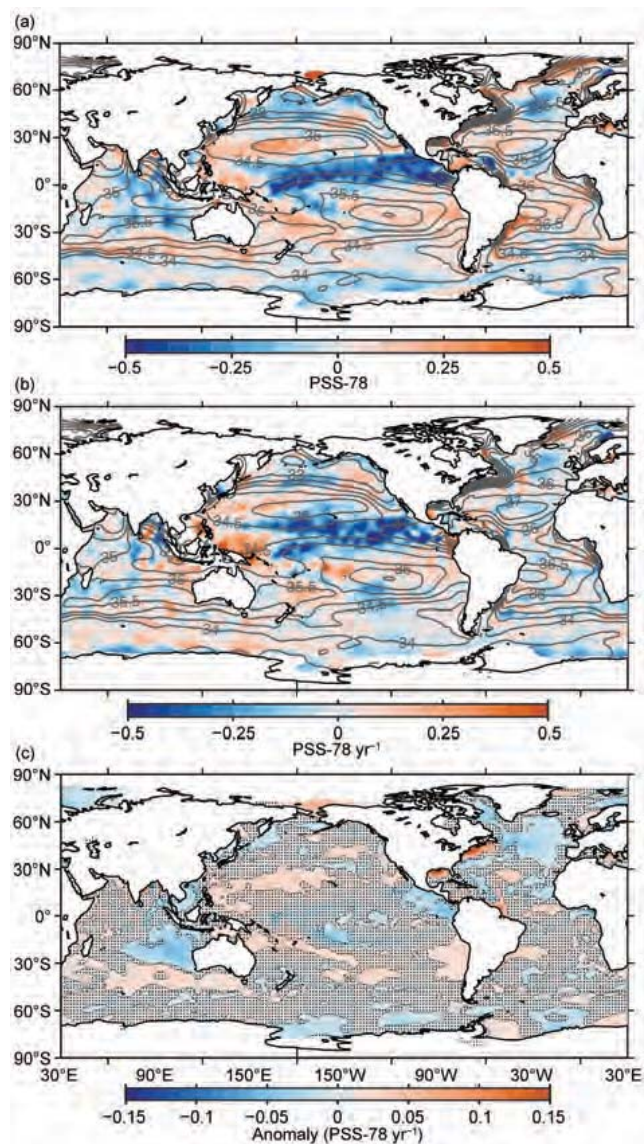


FIG 3.7. (a) Map of the 2015 annual surface salinity anomaly (colors in PSS-78) with respect to monthly climatological salinity fields from *WOA 2009* (yearly average—gray contours at 0.5 PSS-78 intervals). (b) Difference of 2015 and 2014 surface salinity maps [colors in PSS-78 yr⁻¹ to allow direct comparison with (a)]. White ocean areas are too data-poor (retaining < 80% of a large-scale signal) to map. (c) Map of local linear trends estimated from annual surface salinity anomalies for 2005–15 (colors in PSS-78 yr⁻¹). Areas with statistically insignificant trends are stippled. All maps are made using Argo data.

(see Fig. 3.19) of relatively fresh water in the tropical Pacific. The salinification over the tropical warm pool is associated with reduction in freshwater flux anomalies there. These changes are related to the strong El Niño event of 2015 (section 4b). In the subpolar North Atlantic, there was widespread freshening, strongest south of Iceland, but north of Iceland SSS becomes saltier. In the Indian Ocean, SSS decreased south of India from 2014 to 2015, consistent with the

westward spreading and weakening of the prominent fresh anomaly generated west of Australia circa 2011.

Seasonal variations of SSS anomalies in 2015 (Fig. 3.8) from BASS (Xie et al. 2014) show the buildup of anomalously fresh water associated with the tropical Pacific and western tropical Atlantic ITCZs (including just offshore of the Orinoco and Amazon Rivers), the increase in SSS in the tropical warm pool, and the decrease in fresh anomalies under the South Pacific convergence zone (SPCZ). Despite the lower accuracies of the satellite data relative to that of the Argo data, their higher spatial and temporal sampling allows higher spatial and temporal resolution maps than are possible using in situ data alone.

Sea surface salinity trends for 2005–15 exhibit striking patterns in all three oceans (Fig. 3.7c). These trends are estimated by local linear fits to annual average SSS maps from Argo data with a starting year of 2005, because that is when Argo coverage became near-global. Near the salinity maxima in each basin (mostly in the subtropics but closer to 30°S in the Indian Ocean), there are regions of increasing salinity, especially in the North Pacific to the west of Hawaii. In contrast, there are regions in the Southern Ocean where the trend is toward freshening. Again, these patterns are reminiscent of the multidecadal changes discussed above and suggest an intensification of the hydrological cycle over the ocean, even over the last 11 years. There is a strong freshening trend in much of the subpolar North Atlantic, roughly coincident with anomalously low upper ocean heat content there (see Fig. 3.4) suggesting an eastward expansion of the subpolar gyre that may be linked to reductions in the AMOC over the past decade (section 3h). In addition to these patterns there is a freshening trend in the eastern Indian Ocean, probably owing to a lingering signature of the strong 2010–12 La Niña, as discussed above. Freshening trends are also apparent in the eastern tropical Pacific and the South China Sea. The region to the northwest of the Gulf Stream is trending saltier, as well as warmer (section 3c).

3) SUBSURFACE SALINITY—J. Reagan, T. Boyer, C. Schmid, and R. Locarnini

Atlantic Ocean basin-average monthly salinity anomalies for 0–1500 m depth displayed a pattern

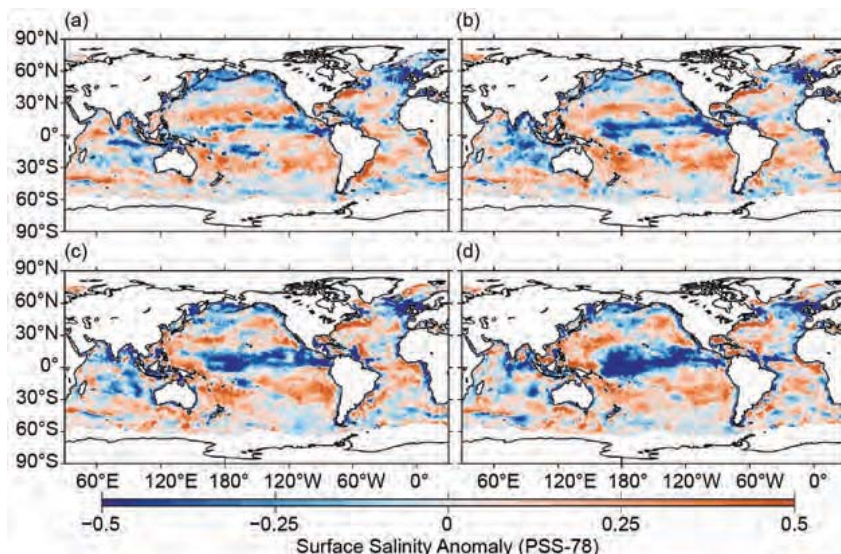


FIG. 3.8. Seasonal maps of SSS anomalies (colors) from monthly blended maps of satellite and in situ salinity data (BASS; Xie et al. 2014) relative to monthly climatological salinity fields from WOA 2009 for (a) Dec–Feb 2014/15, (b) Mar–May 2015, (c) Jun–Aug 2015, and (d) Sep–Nov 2015. Areas with maximum monthly errors exceeding 10 PSS-78 are left white.

during 2015 similar to the previous 10 years, with salty anomalies above 700 m and fresh anomalies below (Fig. 3.9a). From 2014 to 2015 salinity increased in the upper 300 m of the Atlantic, reaching a maximum increase of ~ 0.01 near the surface (Fig. 3.9b). The Pacific Ocean has exhibited fresh anomalies of about -0.02 from 200 to 500 m over the last five years (Fig. 3.9c). However, the upper 75 m was about -0.04 fresher in 2015, in contrast to salty conditions there from mid-2008 to mid-2014. This change reflects the enhanced precipitation along the ITCZ (see Fig. 3.12d) and anomalous eastward equatorial currents (see Fig. 3.19) during the 2015 El Niño (see section 4b). Salty anomalies from 100 to 200 m have been present since 2011. From 2014 to 2015 the Pacific (Fig. 3.9d) freshened in the upper 75 m, approaching about -0.03 at 30 m, and became saltier from 100 to 200 m, approaching ~ 0.01 at 125 m. The Indian Ocean continued to show similar salinity anomaly structure to that of the previous two years, with a fresh surface anomaly from 0 to 75 m, salty subsurface anomaly from 100 to 300 m, a slightly fresh anomaly (maximum of about -0.01) from 400 to 600 m, and a slightly salty anomaly (maximum of ~ 0.01) from 600 to 800 m (Fig. 3.9e). From 2014 to 2015 there was weak freshening (maximum of about -0.01 at 50 m) near the surface and salinification from 100 to 200 m, with a maximum of ~ 0.014 at 150 m (Fig. 3.9f).

North Atlantic 2015 volume-weighted salinity anomalies from 0 to 1500 m (Fig. 3.10a) were mostly positive, with values >0.10 along the Gulf Stream. The eastern portion of the subpolar gyre in the North

Atlantic exhibited a large (about -0.10) fresh anomaly. This fresh feature coincided with anomalously cool upper ocean heat content (see Fig. 3.4). The South Atlantic was dominated by positive salinity anomalies in 2015, with fresh anomalies south of 40°S , perhaps reflecting an anomalously northward position of the low salinity subantarctic front. From 2014 to 2015, positive salinity anomalies in the subtropics persisted with little change in strength, while the freshening north of the Azores Islands continued to strengthen (Fig. 3.10b).

The Indian Ocean displayed a dipole of salinity anomalies north of the equator during 2015, with salty anomalies in the Arabian Sea and fresh anomalies in the Bay of Bengal (Fig. 3.10a). Salty anomalies along the equator transitioned to fresh anomalies across the entire basin south of 15°S to 30°S . These fresh anomalies strengthened east of Madagascar from 2014 to 2015 but weakened west of Australia (Fig. 3.10b) as discussed in section 3d2. From 35°S to 50°S there was a transition from salty to fresh salinity anomalies, likely due to the position of the subantarctic front in 2015 (Fig. 3.10a).

The North Pacific, north of 20°N , was dominated by fresh anomalies in 2015; however, in the northeast

Pacific there was a salty anomaly (Fig. 3.10a) in close proximity to a region of anomalously warm SSTs (see Fig. 3.1). The warm SSTs were at least partly due to a persistent atmospheric ridge in the region (Bond et al. 2015). With ridging, less precipitation and more evaporation are expected. This expectation was partially met (see Fig. 3.12) and likely to have been partially responsible for the observed salty anomaly strengthening from 2014 to 2015 (Fig. 3.10b). The subtropical North Pacific was anomalously salty in 2015, contrasting with fresh anomalies along the ITCZ, consistent with the 2015 $P-E$ anomalies (see Fig. 3.12). Salty anomalies were present in the subtropical South Pacific in 2015, with fresh anomalies along the SPCZ. These tropical and subtropical salinity anomaly features were mostly enhanced when compared to 2014, with the exception of a weakening

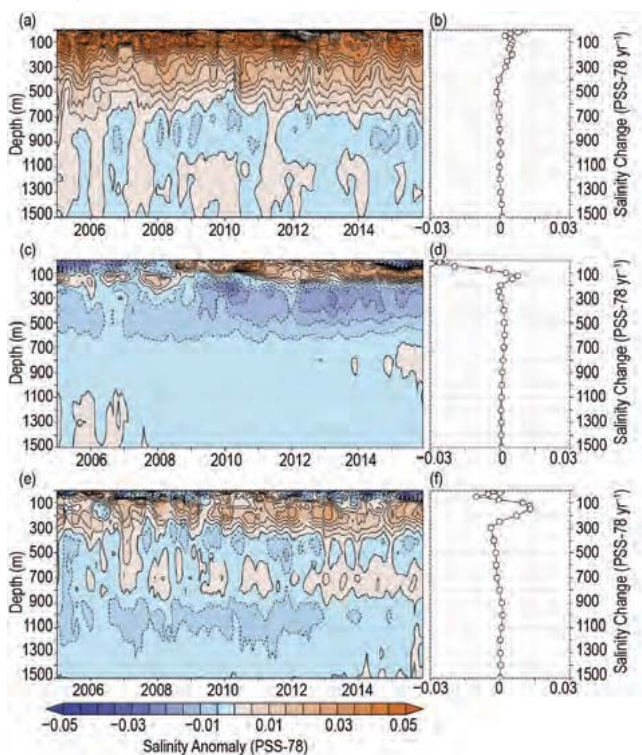


FIG. 3.9. Average monthly salinity anomalies from 0–1500 m for the (a) Atlantic from 2005–15 and (b) the change from 2014 to 2015; (c) Pacific from 2005–15 and (d) the change from 2014 to 2015; and (e) Indian from 2005–15 and (f) the change from 2014 to 2015. Data were smoothed using a 3-month running mean. Anomalies are relative to the long-term WOA 2009 monthly salinity climatology (Antonov et al. 2010).

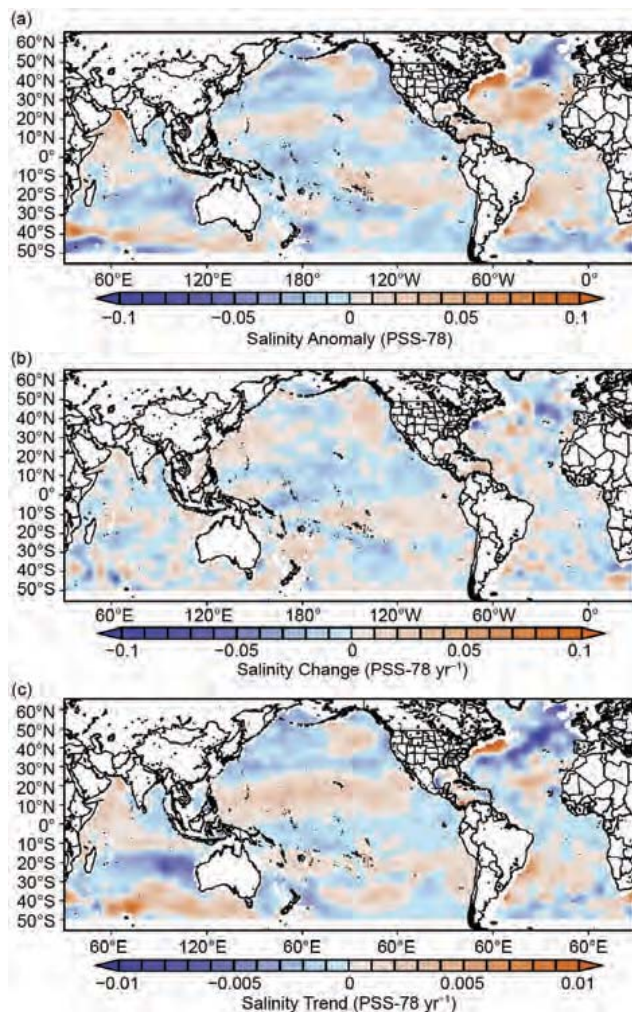


FIG. 3.10. Near-global 0–1500 m volume-weighted salinity anomalies (a) for 2015, (b) change from 2014 to 2015, and (c) linear trend from 2005 to 2015 (yr^{-1}). Anomalies are relative to the long-term WOA 2009 monthly salinity climatology (Antonov et al. 2010). Annual figures were computed by averaging the 12 monthly salinity anomalies over calendar years.

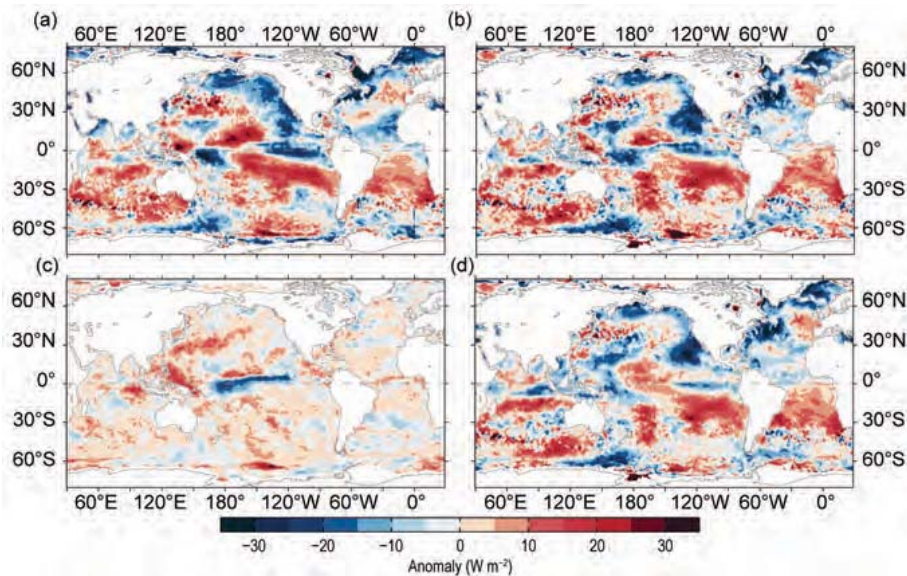


FIG. 3.11. (a) Surface heat flux (Q_{net}) anomalies for 2015 relative to a 5-year (2010–14) mean. Positive values denote ocean heat gain. Panels (b), (c), and (d) are the 2015–2014 anomaly tendencies for Q_{net} , surface radiation (SW+LW), and turbulent heat fluxes (LH+SH), respectively. Positive anomalies denote that the ocean gained more heat in 2015 than in 2014. LH+SH are produced by the OAFIux high-resolution satellite-based analysis, and SW+LW by the NASA FLASHflux project.

positive salinity anomaly over the central subtropical North Pacific in 2015 (Fig. 3.10b). The South Pacific enhancement from 2014 to 2015 is inconsistent with 2015 $P-E$ anomalies (see Fig. 3.12).

The 2005–15 linear trends of the 0–1500 m salinity anomalies (Fig. 3.10c) reveal strong similarities to SSS trends over the same time period (see Fig. 3.7c and discussion above). This match is not surprising as most of the salinity variability from 0 to 1500 m over the global ocean occurs in the upper 300 m (Fig. 3.9). The large ($> -0.01 \text{ yr}^{-1}$) freshening trend in the North Atlantic subpolar gyre could be partially responsible for the observed decline in the strength of the AMOC (Smeed et al. 2014).

e. *Ocean surface heat, freshwater, and momentum fluxes*—
L. Yu, R. F. Adler, G. J. Huffman, X. Jin, S. Kato, N. G. Loeb, P. W. Stackhouse, R. A. Weller, and A. C. Wilber

The ocean and atmosphere communicate via interfacial exchanges of heat, freshwater, and momentum. These air–sea

fluxes are the primary mechanisms for keeping the global climate system in balance with the incoming insolation at Earth’s surface. Most of the shortwave radiation (SW) absorbed by the ocean’s surface is vented into the atmosphere by three processes: longwave radiation (LW), turbulent heat loss by evaporation (latent heat flux, or LH), and turbulent heat loss by conduction (sensible heat flux, or SH). The residual heat is stored in the ocean and transported away by the ocean’s surface circulation, forced primarily by the momentum transferred to the ocean by wind stress. Evaporation connects heat and moisture transfers, and the latter, together with pre-

cipitation, determines the local surface freshwater flux. Identifying changes in the air–sea fluxes is essential in deciphering observed changes in ocean circulation and its transport of heat and salt from the tropics to the poles. In particular, 2015 witnessed the interplay of three different warmings: the warm “Blob” in the

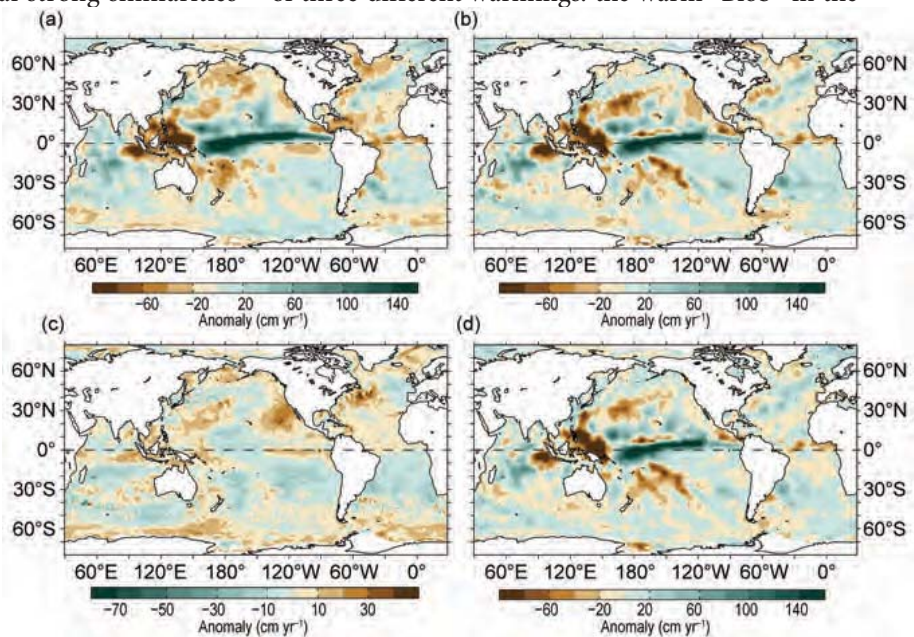


FIG. 3.12. (a) Surface freshwater ($P-E$) flux anomalies for 2015 relative to a 27-year (1988–2014) climatology. 2015–2014 anomaly tendencies for (b) $P-E$, (c) evaporation (E), and (d) precipitation (P), respectively. Green colors denote anomalous ocean moisture gain, and browns denote loss, consistent with the reversal of the color scheme in (c). P is computed from the GPCP version 2.2 product, and E from OAFIux high-resolution satellite-based analysis.